

Article

Surface-Modified Ta₃N₅ Photoanodes for Sunlight-Driven Overall Water Splitting by Photoelectrochemical Cells

Tomohiro Higashi¹, Yutaka Sasaki², Yudai Kawase¹, Hiroshi Nishiyama², Masao Katayama³, Kazuhiro Takanabe¹ and Kazunari Domen^{2,4,*} 

¹ Department of Chemical System Engineering, School of Engineering, The University of Tokyo, 7-3-1 Hongo, Bunkyo-ku, Tokyo 113-8656, Japan; t_higashi@chemsys.t.u-tokyo.ac.jp (T.H.); y_kawase@chemsys.t.u-tokyo.ac.jp (Y.K.); takanabe@chemsys.t.u-tokyo.ac.jp (K.T.)

² Office of University Professors, The University of Tokyo, 7-3-1 Hongo, Bunkyo-ku, Tokyo 113-8656, Japan; y_sasaki@arpchem.t.u-tokyo.ac.jp (Y.S.); nishiyama@arpchem.t.u-tokyo.ac.jp (H.N.)

³ Environmental Science Center, School of Science, The University of Tokyo, 7-3-1 Hongo, Bunkyo-ku, Tokyo 113-8656, Japan; katayama@esc.u-tokyo.ac.jp

⁴ Research Initiative for Supra-Materials, Shinshu University, 4-17-1 Wakasato, Nagano 380-8553, Japan

* Correspondence: domen@chemsys.t.u-tokyo.ac.jp or domen@sinshu-u.ac.jp; Tel.: +81-3-5841-1148

Abstract: The development of visible-light-responsive semiconductor-based photoelectrodes is a prerequisite for the construction of efficient photoelectrochemical (PEC) cells for solar water splitting. Surface modification with an electrocatalyst on the photoelectrode is effective for maximizing the water splitting efficiency of the PEC cell. Herein, we investigate the effects of surface modification of Ta₃N₅ photoanodes with electrocatalysts consisting of Ni, Fe, and Co oxides, and their mixture, on the PEC oxygen evolution reaction (OER) performance. Among the investigated samples, NiFeO_x-modified Ta₃N₅ (NiFeO_x/Ta₃N₅) photoanodes showed the lowest onset potential for OER. A PEC cell with a parallel configuration consisting of a NiFeO_x/Ta₃N₅ photoanode and an Al-doped La₅Ti₂Cu_{0.9}Ag_{0.1}S₅O₇ (LTCA:Al) photocathode exhibited stoichiometric hydrogen and oxygen generation from water splitting, without any external bias voltage. The solar-to-hydrogen energy conversion efficiency (STH) of this cell for water splitting was found to be 0.2% at 1 min after the start of the reaction. In addition, water splitting by a PEC cell with a tandem configuration incorporating a NiFeO_x/Ta₃N₅ transparent photoanode prepared on a quartz insulating substrate as a front-side electrode and a LTCA:Al photocathode as a back side electrode was demonstrated, and the STH was found to be 0.04% at the initial stage of the reaction.

Keywords: photoelectrochemical water splitting; surface modification; solar hydrogen production



Citation: Higashi, T.; Sasaki, Y.; Kawase, Y.; Nishiyama, H.; Katayama, M.; Takanabe, K.; Domen, K. Surface-Modified Ta₃N₅ Photoanodes for Sunlight-Driven Overall Water Splitting by Photoelectrochemical Cells. *Catalysts* **2021**, *11*, 584. <https://doi.org/10.3390/catal11050584>

Academic Editor: Stefano Trocino

Received: 7 April 2021

Accepted: 29 April 2021

Published: 30 April 2021

Publisher's Note: MDPI stays neutral with regard to jurisdictional claims in published maps and institutional affiliations.



Copyright: © 2021 by the authors. Licensee MDPI, Basel, Switzerland. This article is an open access article distributed under the terms and conditions of the Creative Commons Attribution (CC BY) license (<https://creativecommons.org/licenses/by/4.0/>).

1. Introduction

The conversion of solar energy into hydrogen through the photoelectrochemical (PEC) water splitting reaction using semiconductor photoelectrodes is seen as one of the most promising ways to produce chemical fuels that can be stored and are transportable [1–6]. One approach to PEC water splitting involves the use of a PEC cell that combines a photocathode for the hydrogen evolution reaction (HER) and a photoanode for the oxygen evolution reaction (OER) [1,7–9]. This PEC cell can relax the requirements for water splitting, such as the positions of the conduction band minimum and valence band maximum of the individual photoelectrodes [8,9], through a two-step light excitation process. This process makes it possible to drive a spontaneous overall water splitting reaction under simulated sunlight illumination without the application of an external bias voltage.

Two different configurations of PEC cells, consisting of a photoanode–photocathode combination, have been proposed: One is a parallel configuration (parallel PEC cell) where the photoelectrodes are placed side-by-side [8–11]. The other is a tandem configuration (tandem PEC cell) that has a stacked structure, composed of a transparent photoelectrode on

the front side, and a second photoelectrode capable of responding to the light transmitted through the front-side photoelectrode [7,12–14]. Schematic illustrations of the PEC cells are given in Figure S1 in the supporting information (SI). Tandem PEC cells have the potential to achieve high solar-to-hydrogen energy conversion efficiency (STH) values, because the unit area of light illumination is the area of the front-side photoelectrode, leading to potentially increased STH values per unit area. The STH and the working potential (E_{work}) for the PEC cell are determined by photocurrent matching, from the intersection of the current–potential (i - E) curves for the photoanode and photocathode [1,7]. Although overall water splitting by PEC cells has been examined, parallel PEC cells have shown insufficient STH levels—typically less than 2% [8–11,15]. In the case of tandem PEC cells, higher STH values have been reported, but still typically less than 4% [7,12–14,16]. Huang et al. demonstrated an STH of 3.17% using tandem PEC cells consisting of a BiVO_4 -based photoanode and a $\text{Cu}_2\text{ZnSnS}_4$ -based photocathode [14]. In addition, Kobayashi et al. reported an STH of 3.7% using a tandem PEC cell composed of a BiVO_4 -based photoanode and a $\text{CuIn}_{0.5}\text{Ga}_{0.5}\text{Se}_2$ (CIGS)-based photocathode [13].

Ta_3N_5 is considered among the most promising semiconductor photoanodes for PEC oxygen evolution because its band structure is well suited to water splitting [17–19]. A Ta_3N_5 -based photoanode is expected to generate a photocurrent density of 12.9 mA cm^{-2} based on its bandgap of $\sim 2.1 \text{ eV}$ under simulated sunlight, assuming a quantum efficiency of 100% [20]. The theoretical limiting photocurrent density corresponds to an STH value of 15.9% under 1 sun illumination. Despite the promising properties of Ta_3N_5 , instability and a positive onset potential in PEC oxygen evolution are problems to be solved. Surface modification with an electrocatalyst for the OER and insertion of a protective layer have been shown to be effective strategies for enhancing the PEC oxygen evolution efficiency of Ta_3N_5 . Liu et al. demonstrated a photocurrent density of 12.1 mA cm^{-2} at 1.23 V vs. the reversible hydrogen electrode (RHE) under simulated sunlight [20]. This is close to the theoretical maximum photocurrent value for Ta_3N_5 . The authors employed Ta_3N_5 -based photoanodes modified with a hierarchical structure consisting of a TiO_x electron-blocking layer, $\text{FeOOH}/\text{Ni}(\text{OH})_2$ hole-storage layers, and an Ir–Co molecular catalyst for the OER [20]. Nevertheless, the onset potential for PEC oxygen evolution on high-quality Ta_3N_5 was found to be approximately 0.65 V vs. the RHE. This means that application of an external bias voltage is essential to drive PEC water splitting on Ta_3N_5 -based photoanodes.

The intrinsic semiconducting properties of Ta_3N_5 associated with light absorption, extinction via electron–hole pair separation, carrier diffusion, and carrier transport are crucial parameters that affect water splitting efficiency [21]. The crystallinity of Ta_3N_5 is reduced by both bulk and surface defects, which cause the formation of carrier recombination sites and surface states [22–27]. In addition, at the Ta_3N_5 /electrolyte solution interface, the catalytic efficiency of the electrocatalyst and the mass transfer of reactants should also be determined in order to clarify the overall efficiency of water splitting. To date, several electrocatalysts for the OER—such as $\text{Co}(\text{OH})_x$ [28–30], Co_3O_4 [31,32], CoPi [33–35], $\text{Ni}(\text{OH})_x$ [36], and a mixed metal oxide (Ni–Fe–Co) [37,38]—have been used to decorate the surface of Ta_3N_5 , leading to enhanced PEC oxygen evolution efficiency. In these studies, the magnitude of the photocurrent generated at 1.23 V vs. the RHE has mainly been discussed; however, onset potentials have been found around 0.6–0.8 V vs. the RHE [39–41]. Nurlaela et al. demonstrated that the modification with the better OER electrocatalyst improves photocatalytic activity more drastically, in a comparative study of both electrocatalytic and photocatalytic testing using a Ta_3N_5 photocatalyst system [42]. This implies that the onset potential for PEC oxygen evolution on Ta_3N_5 strictly reflects the electrochemical properties of the electrocatalyst that is decorated on the semiconductor surface. Investigations to clarify the impact of the electrocatalyst on PEC oxygen evolution are expected to provide us with strategies to improve the water splitting efficiency, leading to the development of a more efficient PEC cell.

To accomplish overall water splitting with a PEC cell consisting of a photoanode–photocathode combination, photocurrent values at E_{work} of the PEC cell are quite important,

especially in the vicinity of the onset potential of the photoelectrodes. In the present study, we focused on the surface modification of Ta₃N₅ photoanodes as a means of enhancing the efficiency of overall water splitting in the PEC cell. Electrocatalysts such as mono-metal oxides and mixed metal oxides consisting of Ni, Fe, and Co species were loaded onto the surface of Ta₃N₅ photoanodes in order to observe their effect on PEC properties, such as the photocurrent density and onset potential. First, Ta₃N₅ photoanodes prepared on Ta-metal substrates (Ta₃N₅/Ta) were utilized to investigate the effect of different electrocatalysts on PEC oxygen evolution. The electrocatalysts were loaded onto the surface of the Ta₃N₅ through the drop-casting of a non-aqueous solution containing metal-organic precursors, followed by heating in air [43–45]. This surface modification method is relatively simple compared to other modification methods, such as (photo-assisted) electrodeposition. Based on the resulting data, the present study considers overall water splitting using a parallel PEC cell composed of a Ta₃N₅/Ta photoanode and an Al-doped La₅Ti₂Cu_{0.9}Ag_{0.1}S₅O₇ (LTCA:Al) particulate-based photocathode, which has an absorption edge wavelength of 710 nm [9,11]. Next, a transparent Ta₃N₅ photoanode prepared on a double-sided polished quartz insulating substrate (Ta₃N₅/SiO₂) was employed in order to construct the tandem PEC cell. Ta₃N₅/SiO₂ can generate a PEC oxygen evolution via the intrinsic conductivity of the Ta₃N₅ itself, even without using a transparent conductive substrate [43]. The present study considers overall water splitting using a tandem PEC cell composed of a Ta₃N₅/SiO₂ transparent photoanode as the front-side electrode and a LTCA:Al photocathode as the back-side electrode.

2. Results and Discussion

2.1. PEC Characteristics of Surface-Modified Ta₃N₅ Photoanodes

Figure 1 summarizes the photocurrent–potential (*i*-*E*) curves for Ta₃N₅/Ta photoanodes modified with various electrocatalysts (NiFeCoO_{*x*}, NiFeO_{*x*}, CoO_{*x*}, NiO_{*x*}, and FeO_{*x*}) for the OER. Under simulated sunlight illumination, Ta₃N₅/Ta photoanodes produced an anodic photocurrent regardless of the composition of the electrocatalyst. NiFeCoO_{*x*}- and NiFeO_{*x*}-modified Ta₃N₅/Ta photoanodes (NiFeCoO_{*x*}/Ta₃N₅/Ta in Figure 1a and NiFeO_{*x*}/Ta₃N₅/Ta in Figure 1b) clearly exhibited an anodic photocurrent at electrode potentials above 0.6 V vs. the RHE. The photocurrent generated by the NiFeCoO_{*x*}/Ta₃N₅/Ta and NiFeO_{*x*}/Ta₃N₅/Ta photoanodes increased with increasing electrode potential. At electrode potentials below 0.6 V vs. the RHE, these photoanodes did not exhibit any appreciable photocurrent. The photocurrent densities generated by NiFeCoO_{*x*}/Ta₃N₅/Ta and NiFeO_{*x*}/Ta₃N₅/Ta at 1.23 V vs. the RHE were 4.5 mA cm⁻² and 4.0 mA cm⁻², respectively. On the other hand, CoO_{*x*}- and NiO_{*x*}-modified Ta₃N₅/Ta photoanodes (CoO_{*x*}/Ta₃N₅/Ta in Figure 1c and NiO_{*x*}/Ta₃N₅/Ta in Figure 1d) also exhibited an anodic photocurrent at electrode potentials above 0.7 V and 0.8 V vs. the RHE, respectively. For comparison, the previously reported CoP_{*i*}-modified Ta₃N₅/Ta (CoP_{*i*}/Ta₃N₅/Ta) [34] photoanodes also exhibited an anodic photocurrent at electrode potentials above 0.7 V vs. the RHE, in good accordance with the onset potential for the CoO_{*x*}/Ta₃N₅/Ta photoanode. The photocurrent density generated by the CoO_{*x*}/Ta₃N₅/Ta photoanode was found to be 4.5 mA cm⁻² at 1.23 V vs. the RHE, which is comparable to that for the NiFeCoO_{*x*}/Ta₃N₅/Ta photoanode.

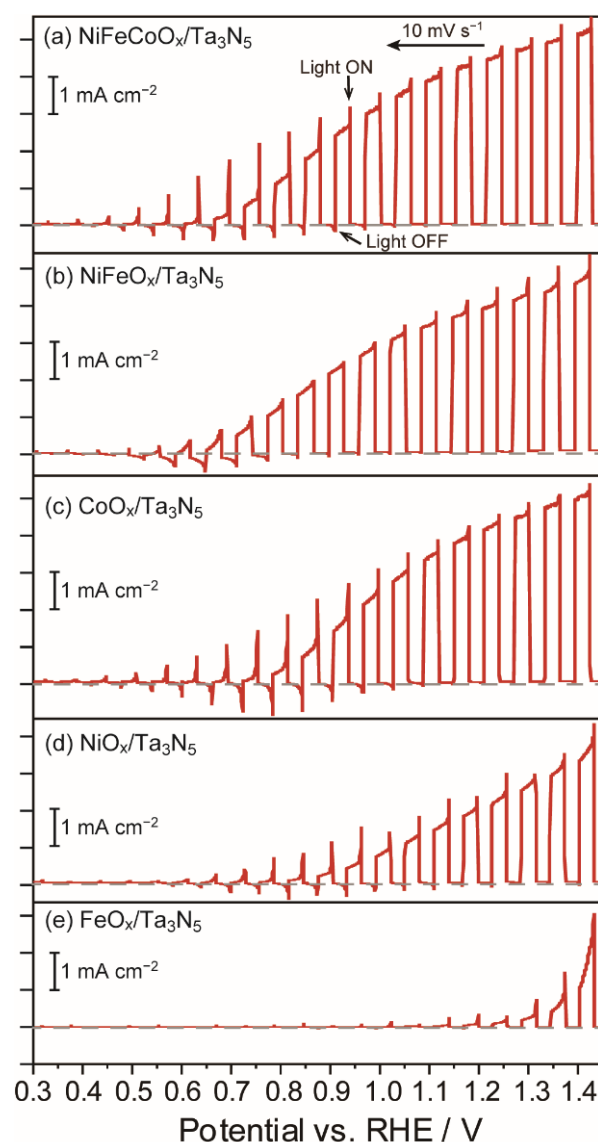


Figure 1. i - E curves obtained from $\text{Ta}_3\text{N}_5/\text{Ta}$ photoanodes modified with electrocatalysts: (a) NiFeCoO_x , (b) NiFeO_x , (c) CoO_x , (d) NiO_x , and (e) FeO_x in 0.1 M sodium phosphate aqueous solution with pH adjusted to 13 by NaOH addition under simulated sunlight (1 sun, AM 1.5G). The potential sweep rate (v) and intermittent irradiation period were 10 mV s^{-1} and 6 s, respectively.

Surface modification with NiFeCoO_x and NiFeO_x electrocatalysts significantly improved the photocurrent at around 0.7 V vs. the RHE, which is the expected E_{work} value for the PEC cell. The cathodic shift of the onset potential is consistent with the lower overpotential for the mixed metal oxide catalysts (NiFeO_x and NiFeCoO_x) [42,46]. In contrast, the photocurrent generated by the $\text{NiO}_x/\text{Ta}_3\text{N}_5/\text{Ta}$ photoanode increased linearly as a function of photoelectrode potential, indicating that the hole-transfer efficiency for NiO_x at the solid/liquid interface is poor compared to that for the mixed metal oxide electrocatalysts (NiFeO_x and NiFeCoO_x). As shown in Figure 1e, the FeO_x -modified $\text{Ta}_3\text{N}_5/\text{Ta}$ ($\text{FeO}_x/\text{Ta}_3\text{N}_5/\text{Ta}$) photoanode shows a low photocurrent of less than 0.1 mA cm^{-2} at 1.23 V vs. the RHE. Note that the i - E curve obtained for $\text{FeO}_x/\text{Ta}_3\text{N}_5/\text{Ta}$ photoanodes shows a low anodic photocurrent compared to that for a bare $\text{Ta}_3\text{N}_5/\text{Ta}$ photoanode (see Figure S2 in the SI), indicating that the FeO_x catalyst did not act effectively as an electrocatalyst for the OER under the present conditions. It should be noted that the visible-light absorption of FeO_x in the present loading amount is negligible (see Figure S3 in the SI), indicating that light

blocking by the FeO_x is not a cause of the poor PEC performance of the $\text{FeO}_x/\text{Ta}_3\text{N}_5/\text{Ta}$ photoanode.

Figure 2 shows typical current-time (i - t) curves for $\text{NiFeCoO}_x/\text{Ta}_3\text{N}_5/\text{Ta}$, $\text{NiFeO}_x/\text{Ta}_3\text{N}_5/\text{Ta}$ and $\text{CoO}_x/\text{Ta}_3\text{N}_5/\text{Ta}$ photoanodes recorded at 0.7 V vs. the RHE under simulated sunlight. Note that because $\text{NiO}_x/\text{Ta}_3\text{N}_5/\text{Ta}$ and $\text{FeO}_x/\text{Ta}_3\text{N}_5/\text{Ta}$ did not generate a meaningful anodic photocurrent at 0.7 V vs. the RHE, evaluation results for these photoanodes are not shown here. After the start of light illumination, a spike-like decrease in photocurrent was observed over a period of several seconds. This was at least partially attributable to double-layer charging by a non-Faradaic process. To accurately evaluate the PEC oxygen evolution, the photocurrent observed 1 min after the start of light illumination will be discussed. The $\text{NiFeCoO}_x/\text{Ta}_3\text{N}_5/\text{Ta}$ photoanode produced a photocurrent density of approximately 0.37 mA cm^{-2} at 1 min after the start of light illumination; however, the photocurrent decreased with time, and was 0.28 mA cm^{-2} after 5 min. On the other hand, the $\text{NiFeO}_x/\text{Ta}_3\text{N}_5/\text{Ta}$ photoanode showed an initial photocurrent density of 0.40 mA cm^{-2} , and maintained a value of 0.38 mA cm^{-2} after 5 min had passed. Haleem et al. reported that Ni-Fe-Co mixed metal oxide-modified Ta_3N_5 photoanodes showed a stable photocurrent of 4 mA cm^{-2} at 1.23 V vs. the RHE for over 2 h [37]. The difference in current stability is most likely caused by the different preparation protocol used in that study, which adopted photo-electrodeposition for the loading of Ni-Fe-Co oxide on Ta_3N_5 . $\text{CoO}_x/\text{Ta}_3\text{N}_5/\text{Ta}$ photoanodes showed an anodic photocurrent of 0.03 mA cm^{-2} , which is clearly lower than the values for $\text{NiFeCoO}_x/\text{Ta}_3\text{N}_5/\text{Ta}$ and $\text{NiFeO}_x/\text{Ta}_3\text{N}_5/\text{Ta}$ photoanodes. Judging from the i - E and i - t characteristics of the surface-modified $\text{Ta}_3\text{N}_5/\text{Ta}$ photoanodes, the $\text{NiFeO}_x/\text{Ta}_3\text{N}_5/\text{Ta}$ photoanode appears promising for the construction of PEC cells for overall water splitting. Therefore, the $\text{NiFeO}_x/\text{Ta}_3\text{N}_5/\text{Ta}$ photoanodes were selected for further study.

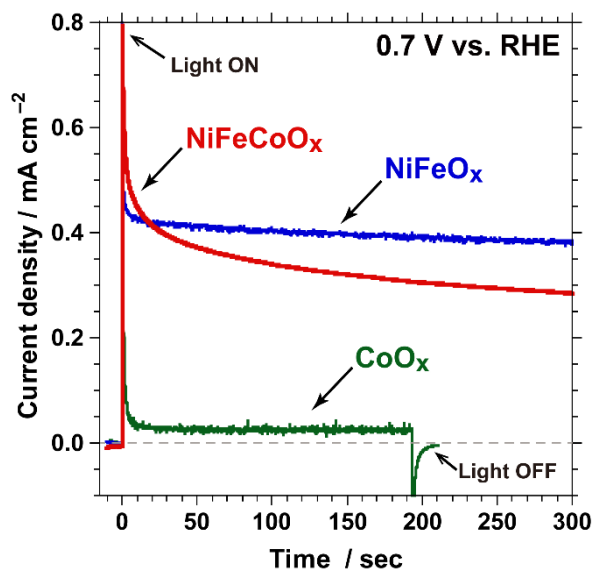


Figure 2. i - t curves recorded at 0.7 V vs. the RHE for $\text{NiFeCoO}_x/\text{Ta}_3\text{N}_5/\text{Ta}$ (red), $\text{NiFeO}_x/\text{Ta}_3\text{N}_5/\text{Ta}$ (blue), and $\text{CoO}_x/\text{Ta}_3\text{N}_5/\text{Ta}$ (green) photoanodes in 0.1 M sodium phosphate aqueous solution with pH adjusted to 13 by NaOH addition under simulated sunlight (1 sun, AM 1.5G).

Figure 3 shows the wavelength dependence of the incident photon-to-current conversion efficiency (IPCE) for $\text{NiFeO}_x/\text{Ta}_3\text{N}_5/\text{Ta}$ photoanodes recorded at 0.7, 0.9, and 1.1 V vs. the RHE. The IPCE spectra demonstrate that $\text{NiFeO}_x/\text{Ta}_3\text{N}_5/\text{Ta}$ photoanodes can generate a photocurrent under light illumination up to a wavelength of 600 nm, which corresponds to the absorption edge wavelength for Ta_3N_5 . Generally, the IPCE increased as the wavelength decreased and the electrode potential became more positive, because of the shorter light penetration depth and the wider depletion layer at the solid/liquid

interface. For illumination with 420 nm monochromatic light, the IPCEs at 0.7, 0.9, and 1.1 V vs. the RHE were found to be 8%, 32%, and 52%, respectively. Intriguingly, the IPCE values at 0.7 V and 1.1 V were comparable at the wavelength of 580 nm, indicating that most of the photocurrent originated from energy conversion utilizing visible light in the short wavelength region.

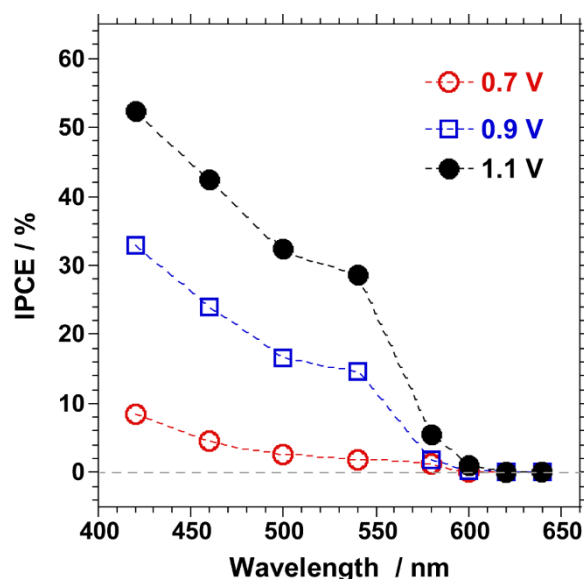


Figure 3. IPCE for the NiFeO_x/Ta₃N₅/Ta photoanode in 0.1 M sodium phosphate aqueous solution at pH 13 recorded at 0.7 V vs. the RHE (open circles), 0.9 V vs. the RHE (open squares) and 1.1 V vs. the RHE (closed circles) as function of wavelength.

As shown in Figure S4 in the SI, SEM images revealed NiFeO_x deposited on the Ta₃N₅ surface, while part of the exposed surface of Ta₃N₅ was clearly observed, indicating that a boundary was formed between the NiFeO_x-covered part and the exposed part of the Ta₃N₅. SEM energy-dispersive X-ray spectroscopic analysis showed that the elements of Ni, Fe, and O attributable to NiFeO_x were distributed on the Ta₃N₅, but the exposed Ta₃N₅ not covered by NiFeO_x was also observed (see Figure S5 in the SI). These results suggest that the exposed Ta₃N₅ causes the decrease in photocurrent with time, partially due to the self-oxidation of Ta₃N₅ under light illumination [31,43,44]. XPS spectra revealed that the Ta₃N₅ surface was covered with NiFeO_x, as Ni and Fe peaks were observed, unlike in the case of the XPS spectra of bare Ta₃N₅/Ta (see Figure S6 in the SI). The XPS data also indicated that NiFeO_x covers the Ta₃N₅ surface, since the Ta and N peak intensities weakened after NiFeO_x modification. Nevertheless, the XPS peaks due to N and Ta were clearly observed even after NiFeO_x modification. This indicates that the Ta₃N₅ surface is partially exposed, in accordance with the SEM results.

2.2. Overall Water Splitting by Parallel PEC Cell

Since the NiFeO_x/Ta₃N₅/Ta photoanode can generate an appreciable anodic photocurrent at 0.7 V vs. the RHE, it is possible to achieve spontaneous overall water splitting without the application of an external bias voltage, using only an appropriate photocathode with an onset potential more positive than 0.7 V vs. the RHE. In the present study, NiFeO_x/Ta₃N₅/Ta and Al-doped La₅Ti₂Cu_{0.9}Ag_{0.1}S₅O₇ (LTCA:Al) were employed as the photoanode and photocathode for a parallel PEC cell (see Figure S7 in the SI). The LTCA:Al photocathode surface was modified with a Pt catalyst in order to promote the HER, and then sequentially modified with a TiO₂ protection layer and a CdS layer in order to promote charge separation through the formation of p–n junctions. This was done because the LTCA:Al modified with Pt, TiO₂, and CdS (Pt/TiO₂/CdS/LTCA:Al) photocathode is capable of driving PEC hydrogen evolution with an onset potential of 0.9 V vs. the RHE

in a highly alkaline aqueous solution in a stable manner. The details of the preparation and the PEC properties of the surface-modified LTCA:Al photocathode have been reported elsewhere [9,11].

Figure 4a shows the i - E curves for a $\text{NiFeO}_x/\text{Ta}_3\text{N}_5/\text{Ta}$ photoanode with a geometrical electrode area of 0.7 cm^2 and an LTCA:Al photocathode with a geometrical electrode area of 0.6 cm^2 under simulated sunlight. In principle, the E_{work} and STH for the PEC cell should be determined by current matching; thus, the operational photocurrent and the E_{work} for this cell were expected to be 0.22 mA and 0.68 V vs. the RHE, respectively. It should be noted that the total geometrical electrode area (1.30 cm^2) for both photoelectrodes must be considered when calculating the photocurrent density and STH values.

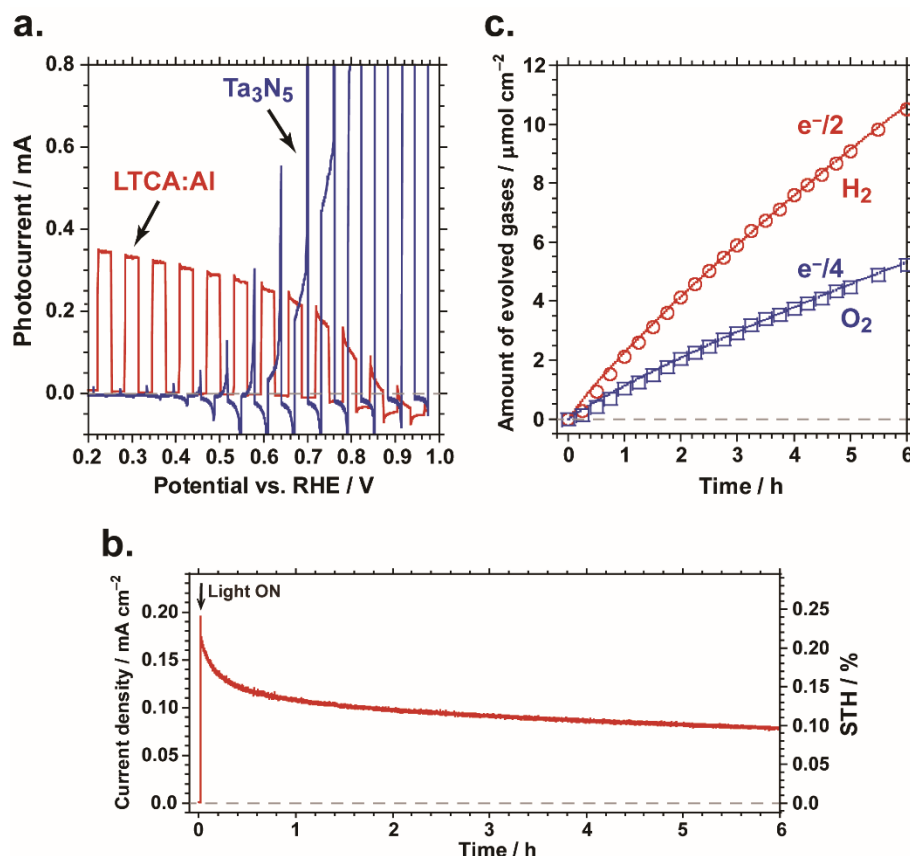


Figure 4. (a) i - E curves for a $\text{NiFeO}_x/\text{Ta}_3\text{N}_5/\text{Ta}$ photoanode (geometrical electrode area: 0.70 cm^2) and a $\text{Pt}/\text{TiO}_2/\text{CdS}/\text{LTCA}:\text{Al}$ photocathode (geometrical electrode area: 0.60 cm^2) in 0.1 M sodium phosphate aqueous solution at pH 13 under simulated sunlight (1 sun, AM 1.5G). The potential sweep rate (v) and the intermittent irradiation period were 10 mV s^{-1} and 6 s , respectively. (b) i - t curve and (c) gas evolution over time for a parallel PEC cell composed of a $\text{NiFeO}_x/\text{Ta}_3\text{N}_5/\text{Ta}$ photoanode and a $\text{Pt}/\text{TiO}_2/\text{CdS}/\text{LTCA}:\text{Al}$ photocathode in 0.1 M sodium phosphate aqueous solution with pH adjusted to 13 under simulated sunlight (1 sun, AM 1.5G), without the application of external bias voltage. The symbols represent the gas quantities determined by GC, while the solid lines indicate the values calculated from the photocurrent.

Figure 4b shows the time course of the photocurrent density for the non-biased parallel PEC cell. The photocurrent density at 1 min after starting the reaction was found to be 0.17 mA cm^{-2} , which corresponds to an STH of 0.2% . Although the photocurrent density for the PEC cell gradually decreased with time, the photocurrent and STH remained 0.08 mA cm^{-2} and 0.1% , respectively, even after 6 h of illumination. The E_{work} value for the PEC cell 1 min after initiating reaction was found to be 0.67 V vs. the RHE, as shown in Figure S8 in the SI. The E_{work} value gradually shifted to more positive potentials over time, reaching 0.7 V vs. the RHE after 6 h. This shift in E_{work} during the water splitting reaction

suggests that the decrease in photocurrent for the PEC cell is attributable to degradation of the NiFeO_x/Ta₃N₅/Ta photoanode rather than degradation of the Pt/TiO₂/CdS/LTCA:Al photocathode. The detachment of the NiFeO_x electrocatalyst on the Ta₃N₅ surface is one possible reason for the gradual decrease in the photocurrent of the Ta₃N₅/Ta photoanode. The photocurrent density at around 0.7 V vs. the RHE decreased significantly after the water splitting reaction (see Figure S9 in the SI). A partial removal of NiFeO_x from the photoanode surface, giving rise to a decrease in the surface coverage of the NiFeO_x, was revealed by the results of the SEM observation after the water splitting reaction (see Figure S10 in the SI).

Hydrogen and oxygen were generated by the parallel PEC cell at a stoichiometric ratio of 2:1 over 6 h, as shown in Figure 4c. The amounts of evolved hydrogen and oxygen were consistent with the values calculated from the total charge calculated from the recorded photocurrent, indicating that the Faradaic efficiency for overall water splitting for the cell is ~97%. We note that the apparent delay in gas detection for the initial 1 h is due to the time required for homogenization of the gas phase in the measurement system. The average gas generation rates over the 6 h period were approximately 1.8 μmol cm⁻² h⁻¹ for hydrogen and 0.9 μmol cm⁻² h⁻¹ for oxygen. The hydrogen and oxygen generation rates were approximately 1.6 times higher than those previously reported for a parallel PEC cell composed of an Ir–Co catalyst-loaded BaTaO₂N photoanode and a Pt/TiO₂/CdS/LTCA:Al photocathode with average gas generation rates of 1.1 μmol cm⁻² h⁻¹ for hydrogen and 0.55 μmol cm⁻² h⁻¹ for oxygen [9]. The slightly higher STH for the parallel PEC cell incorporating the Ta₃N₅–LTCA:Al combination originates from the improved photocurrent for the PEC cells at E_{work} .

2.3. Overall Water Splitting by Tandem PEC Cell

Next, overall water splitting by a tandem PEC cell using surface-modified Ta₃N₅ photoanodes was assessed. In this trial, a transparent Ta₃N₅ photoanode fabricated on an insulating quartz substrate (Ta₃N₅/SiO₂) was employed for the front-side photoanode in the cell. The optical characteristics of the Ta₃N₅/SiO₂ transparent photoanodes required tuning, because the water splitting efficiency of the cell is determined by the intensity and the wavelength of the light transmitted through the front-side photoanode. As shown in Figure S11 in the SI, as the thickness of the Ta₃N₅ films increased, the color changed from pale orange to dark red.

Figure 5a shows the UV-vis transmission spectra of the Ta₃N₅/SiO₂ photoanodes with different thicknesses of Ta₃N₅. In the film thickness range of 100–800 nm, these photoanodes showed an optical transmittance of over 60% at wavelengths longer than 600 nm. The fringes observed in the spectra are ascribable to optical interference. The 800 nm thick Ta₃N₅ film absorbed most of the visible light at wavelengths up to 600 nm, which is the absorption edge wavelength for Ta₃N₅. A plot of the absorption coefficient for the Ta₃N₅/SiO₂ photoanode as a function of wavelength is shown in Figure S12a in the SI. The absorption coefficient for Ta₃N₅/SiO₂ appears to monotonically decrease with increasing wavelength. The values are in the order of 10⁵–10⁴ cm⁻¹ in the range 350–600 nm. Ziani et al. reported absorption coefficients for Ta₃N₅ between 8 × 10⁵ and 1 × 10⁴ cm⁻¹ for wavelengths from 300 to 600 nm [27], which are in good agreement with the results of the present study. Figure S12b in the SI displays a plot of light intensity as a function of the optical path length in Ta₃N₅/SiO₂. When Ta₃N₅/SiO₂ is irradiated with light with a wavelength shorter than 450 nm, the light can be completely absorbed by Ta₃N₅ with a thickness of 300 nm. On the other hand, light with wavelengths of 500 and 550 nm is fully absorbed when the Ta₃N₅/SiO₂ is 800 nm thick. This shows that using Ta₃N₅ with a thickness of 800 nm is preferable in order to absorb light at wavelengths relevant to the PEC oxygen evolution on Ta₃N₅/SiO₂ (350–600 nm). Figure S13 in the SI shows the UV-vis transmission spectra of the NiFeO_x-modified Ta₃N₅/SiO₂ photoanodes with 800 nm-thick Ta₃N₅. Even after NiFeO_x modifications, the optical transmittance at wavelengths longer than 600 nm remained over 60%, which can apply to the tandem PEC

cell. Our previous study has demonstrated that an increase in the loading amount of NiFeO_x decreases the transmittance of Ta₃N₅/SiO₂ photoanodes, while enhancing the OER performance of NiFeO_x/Ta₃N₅/SiO₂ [47]. However, when the loading amount of NiFeO_x is larger than 0.1 μmol cm⁻², the PEC performance decreases because of the decrease in the light intensity reaching the Ta₃N₅ [47]. Therefore, Ta₃N₅/SiO₂ photoanodes with the loading amount of 0.03 μmol cm⁻², which is same amount of NiFeO_x in Ta₃N₅/Ta, was employed in order to investigate the PEC performance on Ta₃N₅/SiO₂ photoanodes.

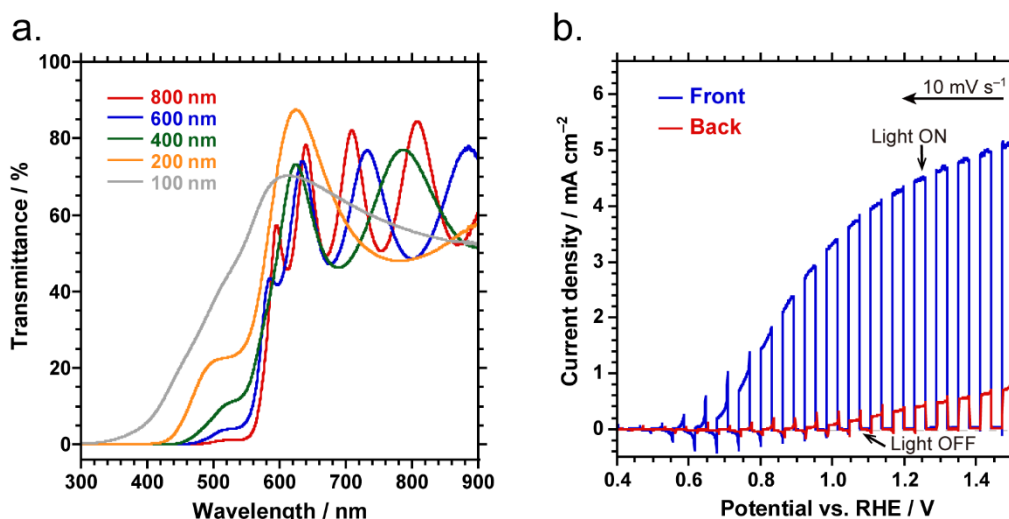


Figure 5. (a) UV-vis transmission spectra for Ta₃N₅/SiO₂ with Ta₃N₅ thicknesses of 100, 200, 400, 600, and 800 nm. (b) *i*-*E* curves for a NiFeO_x/Ta₃N₅/SiO₂ transparent photoanode with 800 nm thick Ta₃N₅ in 0.1 M sodium phosphate aqueous solution with pH 13 by NaOH addition under simulated sunlight (1 sun, AM 1.5G). These curves were obtained via illumination from the front side of the Ta₃N₅ (blue) and from the back side of the SiO₂ substrate (red).

Figure 5b presents typical *i*-*E* curves acquired for NiFeO_x/Ta₃N₅/SiO₂ photoanodes with 800 nm thick Ta₃N₅ under simulated sunlight illumination from the front side (Ta₃N₅) and from the back side (SiO₂). Under light illumination from the front side, the photoanode shows a photocurrent density of 4.4 mA cm⁻² at 1.23 V vs. the RHE. This value is consistent with that for previously reported NiFeO_x-modified Ta₃N₅/SiO₂ photoanodes [43,47]. The *i*-*t* curves for the NiFeO_x/Ta₃N₅/SiO₂ transparent photoanode recorded at 1.23 V vs. the RHE (see Figure S14 in the SI) demonstrate that the initial photocurrent density of 4.4 mA cm⁻² generated by the photoanode was well consistent with photocurrent value on the *i*-*E* curves (Figure 5b). The photocurrent for the NiFeO_x/Ta₃N₅/SiO₂ at 1.23 V vs. the RHE gradually decreased to 70% over 30 min. This gradual decrease of the photocurrent is most likely due to the self-photo-oxidation of the Ta₃N₅ surface [47]. On the other hand, when the light irradiated the electrode from the back side, the photocurrent significantly decreased to 0.4 mA cm⁻² at 1.23 V vs. the RHE. As shown in Figure S15 in the SI, the photocurrent at 1.23 V vs. the RHE tended to increase as the Ta₃N₅ film's thickness increased when irradiation was from the front side. The photocurrent at 0.7 V vs. the RHE which is the expected *E*_{work} of the PEC cell also increased with the increase in the Ta₃N₅ film's thickness. In contrast, when irradiation was from the back side, the photocurrent tended to decrease as the thickness of Ta₃N₅ increased. Light with short wavelengths, such as 350 nm and 400 nm, is completely absorbed within about 100 nm of the SiO₂/Ta₃N₅ interface (see Figure S12b in the SI). This means that the generated carriers need to travel at least 700 nm to reach the Ta₃N₅/electrolyte interface. In addition, the holes generated by shorter wavelength light may not be transferred effectively to the Ta₃N₅/electrolyte interface due to carrier recombination, leading to a decrease in photocurrent. The onset potential, which is the emergence of the anodic photocurrent, clearly shifted from 0.6 V vs. the RHE to 1.0 V vs. the RHE when the illumination direction changed from the front side to the back side.

This result indicates that the light needs to reach the depletion region of Ta_3N_5 in order to cause holes to accumulate at the electrified Ta_3N_5 /electrolyte interface effectively.

Finally, the overall water splitting reaction using a tandem PEC cell composed of a combination of a $\text{NiFeO}_x/\text{Ta}_3\text{N}_5/\text{SiO}_2$ photoanode on top of a $\text{Pt}/\text{TiO}_2/\text{CdS}/\text{LTCA}:\text{Al}$ photocathode is discussed. Based on the aforementioned discussion, a $\text{NiFeO}_x/\text{Ta}_3\text{N}_5/\text{SiO}_2$ photoanode with a Ta_3N_5 thickness of 800 nm was employed as the front-side transparent photoanode in the tandem PEC cell. The $\text{Pt}/\text{TiO}_2/\text{CdS}/\text{LTCA}:\text{Al}$ photocathode has an absorption edge wavelength of 710 nm; thus, this photocathode can exhibit the PEC hydrogen evolution reaction by utilizing the light transmitted through the transparent $\text{NiFeO}_x/\text{Ta}_3\text{N}_5/\text{SiO}_2$ (see Figure S16 in the SI). Figure 6a shows i - E curves for the $\text{NiFeO}_x/\text{Ta}_3\text{N}_5/\text{SiO}_2$ transparent photoanode and the $\text{Pt}/\text{TiO}_2/\text{CdS}/\text{Al}:\text{LTCA}$ photocathode. Note that the photocurrent density of $\text{Pt}/\text{TiO}_2/\text{CdS}/\text{Al}:\text{LTCA}$ photocathode was calculated by dividing the photocurrent value by the geometrical electrode area of the LTCA:Al photocathode (0.26 cm^2). On the other hand, the photocurrent density of the $\text{Pt}/\text{TiO}_2/\text{CdS}/\text{LTCA}:\text{Al}$ photocathode placed behind the $\text{NiFeO}_x/\text{Ta}_3\text{N}_5/\text{SiO}_2$ transparent photoanode was calculated using the geometrical electrode area of Ta_3N_5 (0.67 cm^2) of the front-side electrode. The cathodic photocurrent density at 0.7 V vs. the RHE generated by the $\text{Pt}/\text{TiO}_2/\text{CdS}/\text{LTCA}:\text{Al}$ was reduced to about 25% when it was placed behind the $\text{NiFeO}_x/\text{Ta}_3\text{N}_5/\text{SiO}_2$ photoanode. The intersection of the photocurrent density and the expected E_{work} for the tandem PEC cell were found to be 0.04 mA cm^{-2} and 0.64 V vs. the RHE, respectively.

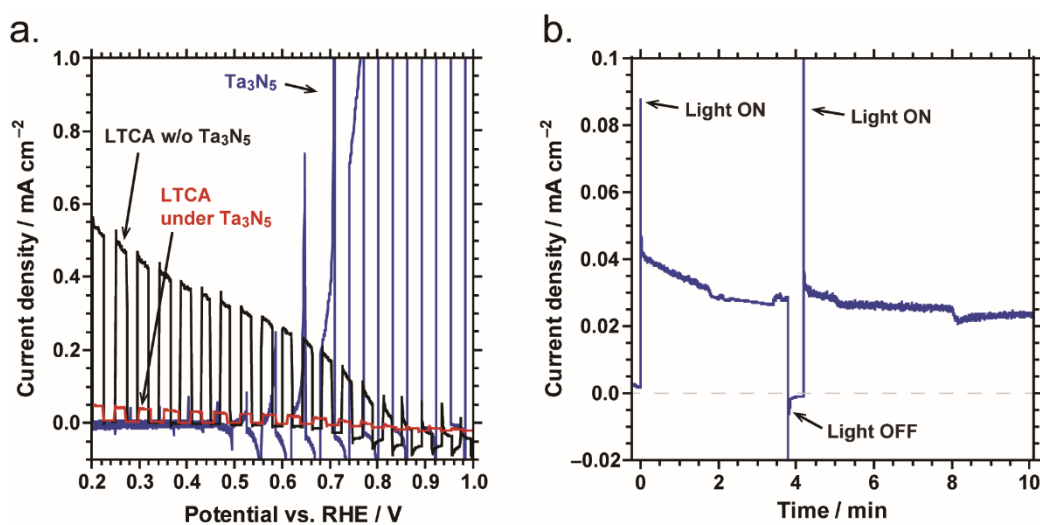


Figure 6. (a) i - E curves for a $\text{NiFeO}_x/\text{Ta}_3\text{N}_5/\text{SiO}_2$ transparent photoanode (geometrical electrode area: 0.67 cm^2) and a $\text{Pt}/\text{TiO}_2/\text{CdS}/\text{LTCA}:\text{Al}$ photocathode (geometrical electrode area: 0.26 cm^2), with and without (w/o) the $\text{Ta}_3\text{N}_5/\text{SiO}_2$ photoanode. (b) i - t curves for a tandem PEC cell composed of a $\text{NiFeO}_x/\text{Ta}_3\text{N}_5/\text{SiO}_2$ transparent photoanode and a $\text{Pt}/\text{TiO}_2/\text{CdS}/\text{LTCA}:\text{Al}$ photocathode under simulated sunlight (1 sun, AM 1.5G) without the application of external bias voltage in 0.1 M sodium phosphate aqueous solution with pH adjusted to 13.

Figure 6b shows the time course of the photocurrent generated by the non-biased tandem PEC cell. The tandem cell generates a photocurrent of 0.036 mA cm^{-2} under continuous light illumination, which is in relatively good agreement with the expected photocurrent estimated from the intersection of the i - E curves (see Figure 6a). The photocurrent density of 0.036 mA cm^{-2} corresponds to an STH of 0.04%, assuming that the Faradaic efficiency for water splitting is 100%. The photocurrent generated by the tandem PEC cell decreased over time, and the photocurrent after 10 min of reaction was found to be 0.02 mA cm^{-2} . Akagi et al. reported an STH of approximately 0.06% for overall water splitting by a tandem PEC cell composed of a Mg-doped Ta_3N_5 transparent photoanode fabricated on a conductive carbon nanotube-coated quartz substrate and a solid solution ZnSe-CIGS-based photocathode with an absorption edge wavelength of 900 nm [40]. Al-

though the present results are comparable with those for the previously reported tandem PEC cell using a transparent Ta₃N₅-based photoanode, the use of Ta₃N₅ prepared directly on an insulating substrate made it possible to construct the current tandem PEC cell. Our results represent progress in the development of tandem PEC cells that combine a metal oxysulfide-based particulate photocathode and a nitride-based transparent photoanode prepared on an insulator. This will further expand the list of potential narrow bandgap materials applicable to the construction of tandem-type PEC cells.

3. Materials and Methods

3.1. Preparation of Ta₃N₅-Based Photoanodes

A Ta₃N₅ thin film was prepared following previously reported methods [34]. An approximately 500 nm-thick TaO_δ film was deposited on mirror-polished Ta substrates (10 × 10 × 0.3 mm) via radio frequency (RF) magnetron sputtering (ES-205L, Eiko, Tokyo, Japan). The sputtering target was a Ta metal disk (3N pure (99.9%), Kojundo Chem. Lab. Co., Saitama, Japan) 60 mm in diameter and 3 mm thick. The Ta target was pre-sputtered in an Ar gas atmosphere for 10 min in order to clean its surface. A gas purifier (VICI Metronics Inc., Poulsbo, Washington, USA) was connected to the incoming Ar line in order to eliminate impurities. The base pressure in the sputtering chamber was 3 × 10⁻⁷ Pa. The precursor films were prepared at an RF power of 70 W for 2.5 h in Ar at a 4.0 Pa working pressure. The resulting films were subsequently heated at 1073 K for 1 h in a flow of NH₃ (200 sccm) with a temperature ramp of 10 K min⁻¹. In addition, Ta₃N₅ thin films were prepared on double-side polished quartz (SiO₂) insulating substrates (10 × 10 × 0.5 mm) following a modified version of previously reported methods [43]. Ta-metal films with thicknesses of 75, 150, 300, 450, and 600 nm were sputtered at an RF power of 70 W in Ar at a working pressure of 3.0 Pa. The sputtering rate for the films under these conditions was 4.0 nm min⁻¹. These precursor films were heated in a flow consisting of a mixture of NH₃ and N₂ (NH₃ = 100 sccm and N₂ = 100 sccm) at 1073 K with a temperature ramp of 10 K min⁻¹. Precursor films with thicknesses of 75, 150, and 300 nm were heated at 1073 K for 0.5 h in order to produce Ta₃N₅ films with thicknesses of 100, 200, and 400 nm, while films with thicknesses of 450 and 600 nm were heated at 1073 K for 1 h in order to produce the 600 nm and 800 nm thick Ta₃N₅.

3.2. Surface Modification of Ta₃N₅-Based Photoanodes

Metal oxide catalysts to promote the OER were deposited on the surface of Ta₃N₅. Deposition was accomplished by combining precursor solutions of iron(III) 2-ethylhexanoate (Wako Chemicals, Richmond, VA, USA), nickel(II) 2-ethylhexanoate (Wako), and Co(III) 2-ethyl hexanoate (Wako) dissolved in hexane (HPLC grade, Wako). The precursor solutions of FeO_x, NiO_x, CoO_x, NiFeO_x, and NiFeCoO_x were prepared as follow: For the mono-metal oxide catalysts (FeO_x, NiO_x, and CoO_x), 10 μL of metal complex was added to 10 mL of hexane, and then 40 μL of this solution was drop-cast on the surface of the Ta₃N₅ surface, with a coverage area of approximately 0.7 cm². For the mixed metal oxide catalysts (NiFeO_x and NiFeCoO_x), 10 μL of each metal complex was added to 10 mL of hexane, and then 20 μL of the solutions were drop-cast on the Ta₃N₅ surface, with a coverage area of approximately 0.7 cm². The loading amount of these catalysts was 0.03 μmol cm⁻². This was followed by heating at 413 K in air for 45 min. Subsequently, the samples were rinsed with a copious amount of hexane in order to remove residual precursors, followed by drying in air. Indium metals were soldered onto the back side of Ta substrate of Ta₃N₅/Ta and onto the edge of the Ta₃N₅ surface of the Ta₃N₅/SiO₂. Following this, additional indium was soldered to connect the lead wire, and then the unused region was covered with epoxy resin as insulation. The schematic illustration of the Ta₃N₅/Ta and Ta₃N₅/SiO₂ is given in Figure S17 in the SI.

3.3. Characterization

Samples were characterized using UV-vis transmission spectroscopy (V-670, JASCO Co., Tokyo, Japan), scanning electron microscopy (SEM, SU8020, HITACHI Ltd., Tokyo, Japan), and X-ray photoelectron spectroscopy (XPS, JPS-9000, JEOL Ltd., Tokyo, Japan) using MgK α radiation, while the binding energy scale was calibrated using the C1s peak at 285.0 eV.

3.4. PEC Measurements

PEC measurements for the Ta₃N₅-based photoanodes were performed with a three-electrode configuration using a Ag/AgCl/sat'd KCl reference electrode and a coiled Pt wire counter electrode. The electrode potential was controlled using a potentiostat (HSV-110, Hokuto Denko Corp., Tokyo, Japan). A surface-modified Ta₃N₅ photoanode with an exposed area of 0.7 to 0.5 cm² was positioned in a glass cell containing 0.1 M sodium phosphate aqueous solution with the pH adjusted to 13 by the addition of NaOH as the electrolyte. The electrode potentials were converted to values versus the reversible hydrogen electrode (vs. the RHE) using the Nernst equation. A solar simulator equipped with an AM 1.5G filter (XES-40S2, SAN-EI Electric Co. Ltd., Osaka, Japan) was employed as the light source. The intensity of the light was adjusted to AM 1.5G with 100 mW cm⁻². Incident photon-to-current conversion efficiency (IPCE) values were obtained using a MAX-302 Xe light source (Asahi Spectra Co. Ltd., Tokyo, Japan) equipped with bandpass filters to provide monochromatic light. IPCEs were calculated using the equation:

$$\text{IPCE (\%)} = [(1240/\lambda) \times J/P] \times 100, \quad (1)$$

where λ is the wavelength of the monochromatic incident light (nm), J is the photocurrent density (mA cm⁻²), and P is the intensity of the incident light (mW cm⁻²).

Overall water splitting was performed in two differently configured PEC cells consisting of a Ta₃N₅ photoanode and an LTCA:Al photocathode. For the parallel PEC cell, the surface-modified Ta₃N₅/Ta photoanode and the LTCA:Al photocathode were placed side-by-side. For the tandem PEC cell, the surface-modified Ta₃N₅/SiO₂ transparent photoanode was placed in front of the LTCA:Al photocathode. The Ta₃N₅-based photoanode and the LTCA:Al-based photocathode were connected to one another via lead wires. The LTCA:Al photocathode was prepared using the particle transfer method [9,11,48]. Prior to the construction of the cells, the LTCA:Al photocathodes were sequentially modified with a CdS layer via chemical bath deposition, a TiO₂ surface protection layer was deposited via drop-casting of a tetraisopropyl orthotitanate aqueous solution, and a Pt catalyst was deposited via photoelectrochemical deposition [9]. The resulting photocurrent and quantities of evolved gases were simultaneously determined using a multimeter and a micro gas chromatograph (GC3000A, Agilent Technologies Inc. Santa Clara, CA, USA).

The STH values for the cells were calculated from the i - t curves for the PEC cells using the following equation [44]:

$$\text{STH (\%)} = J \times 1.23 \text{ V} \times 100/P, \quad (2)$$

where J is the photocurrent density (mA cm⁻²) and P is the intensity of simulated sunlight (AM 1.5G, 100 mW cm⁻²). Note that the geometrical electrode areas for the parallel PEC cell and the tandem PEC cell were the total effective area of both photoelectrodes (Ta₃N₅-LTCA:Al) and the effective area of the front-side Ta₃N₅ photoanode, respectively.

4. Conclusions

The surface of Ta₃N₅ thin film-based photoanodes was modified with electrocatalysts consisting of metal oxides in order to clarify their effect on the PEC oxygen evolution efficiency. Surface modification with mixed metal oxides such as NiFeO_x and NiFeCoO_x improved the onset potential to 0.6 V vs. the RHE, while the photoanodes with surface modification by the mono-metal oxides—namely, NiO_x, FeO_x, and CoO_x—exhibited poor

onset potentials as high as 0.7 V vs. the RHE. This trend for the onset potential is attributable to the overpotential for the electrocatalytic OER performance of the applied materials. The NiFeO_x/Ta₃N₅ photoanode exhibited a significantly enhanced photocurrent, achieving a value of 0.40 mA cm⁻² at 0.7 V vs. the RHE. A parallel PEC cell composed of a NiFeO_x/Ta₃N₅ photoanode and a Pt/TiO₂/CdS/LTCA:Al photocathode exhibited non-biased, spontaneous overall water splitting, with stoichiometric hydrogen and oxygen evolution, and a Faradaic efficiency of ~97%. The STH for the parallel PEC cell was found to be 0.2% after 1 min of simulated sunlight illumination. A tandem PEC cell composed of a NiFeO_x/Ta₃N₅/SiO₂ transparent photoanode as the front-side electrode and a Pt/TiO₂/CdS/LTCA:Al photocathode behind it generated a self-standing photocurrent density of 0.036 mA cm⁻² without the application of an external bias voltage. The feasibility of water splitting by tandem PEC cells consisting of a nitride-based transparent photoanode and an oxysulfide-based particulate photocathode was established in the present study. The photocurrent density and the STH value obtained by the tandem PEC cells are far from sufficient for practical applications, and are lower than those reported for PEC cells. There are still many problems to be solved, such as the low photocurrent at electrode potentials below 0.7 V vs. the RHE, and the low stability of the Ta₃N₅ photoanodes. The photocurrent can be enhanced by further surface modification and improvement of the semiconductor properties of Ta₃N₅. Introducing an oxide-based protective layer on the NiFeO_x electrocatalyst might be helpful in stabilizing the Ta₃N₅ photoanode. Further improvement of the performance of the photocathode and the tandem PEC cell, enabling us to accurately evaluate the gas generation rates and the Faradaic efficiency, are also issues for future work.

Supplementary Materials: The following are available online at <https://www.mdpi.com/article/10.3390/catal11050584/s1>, Figure S1: schematic illustration of PEC cells consisting of photoanode–photocathode combinations; Figure S2: *i*-*E* curve for a bare Ta₃N₅ photoanode; Figure S3: UV-vis transmission spectrum of an FeO_x-deposited quartz substrate; Figure S4: SEM images; Figure S5: SEM–EDX analysis; Figure S6: XPS spectra; Figure S7: photograph of a parallel PEC cell; Figure S8: time course of the working potential of a PEC cell; Figure S9: *i*-*E* curves for a NiFeO_x/Ta₃N₅ photoanode after water splitting reaction; Figure S10: SEM images after water splitting reaction; Figure S11: photograph of a Ta₃N₅/SiO₂ photoanode; Figure S12: absorption coefficient spectrum and plot of light intensity as function of optical path length in Ta₃N₅; Figure S13: UV-vis transmission spectrum for a NiFeO_x/Ta₃N₅/SiO₂ transparent photoanode; Figure S14: *i*-*t* curve for a NiFeO_x/Ta₃N₅/SiO₂ transparent photoanode at 1.23 V vs. the RHE; Figure S15: *i*-*E* curves for Ta₃N₅/SiO₂ transparent photoanodes with different film thicknesses; Figure S16: photograph of a tandem PEC cell; Figure S17: schematic illustration of the cross-sectional structures of Ta₃N₅/Ta and Ta₃N₅/SiO₂ photoanodes.

Author Contributions: T.H., Y.S. and Y.K. prepared the Ta₃N₅-based photoanodes and conducted PEC oxygen evolution reactions under simulated sunlight; T.H. constructed PEC cells composed of Ta₃N₅-based photoanodes and LTCA:Al particulate photocathodes, and evaluated the water splitting efficiency of the cells; K.D. and H.N. supervised the experimental work; K.D., H.N., K.T. and M.K. discussed the results; T.H. wrote the manuscript with contributions from the other co-authors. All authors have read and agreed to the published version of the manuscript.

Funding: This work was financially supported by the New Energy and Industrial Technology Development Organization (NEDO) and by the Japan Society for the Promotion of Science (grant number 19K15670).

Data Availability Statement: The data presented in this study are available on requested from the corresponding author.

Acknowledgments: The authors are grateful to A. Furuhi, Y. Shinohara, T. Hisatomi, and T. Minegishi at the University of Tokyo for their assistance in the preparation of the photocatalyst powder. This work was financially supported by the Artificial Photosynthesis Project of the New Energy and Industrial Technology Development Organization (NEDO). This work was also funded in part by a Grant-in-Aid for Early Career Scientists (No. 19K15670) from JSPS.

Conflicts of Interest: The authors declare no conflict of interest.

References

1. Walter, M.G.; Warren, E.L.; McKone, J.R.; Boettcher, S.W.; Mi, Q.; Santori, E.A.; Lewis, N.S. Solar Water Splitting Cells. *Chem. Rev.* **2010**, *110*, 6446–6473. [[CrossRef](#)]
2. Pinaud, B.A.; Benck, J.D.; Seitz, L.C.; Forman, A.J.; Chen, Z.; Deutsch, T.G.; James, B.D.; Baum, K.N.; Baum, G.N.; Ardo, S.; et al. Technical and economic feasibility of centralized facilities for solar hydrogen production via photocatalysis and photoelectrochemistry. *Energy Environ. Sci.* **2013**, *6*, 1983–2002. [[CrossRef](#)]
3. McKone, J.R.; Lewis, N.S.; Gray, H.B. Will Solar-Driven Water-Splitting Devices See the Light of Day? *Chem. Mater.* **2014**, *26*, 407–414. [[CrossRef](#)]
4. Jia, J.; Seitz, L.C.; Benck, J.D.; Huo, Y.; Chen, Y.; Ng, J.W.D.; Bilir, T.; Harris, J.S.; Jaramillo, T.F. Solar water splitting by photovoltaic-electrolysis with a solar-to-hydrogen efficiency over 30%. *Nat. Commun.* **2016**, *7*, 13237. [[CrossRef](#)]
5. Shaner, M.R.; Atwater, H.A.; Lewis, N.S.; McFarland, E.W. A comparative technoeconomic analysis of renewable hydrogen production using solar energy. *Energy Environ. Sci.* **2016**, *9*, 2354–2371. [[CrossRef](#)]
6. Montoya, J.H.; Seitz, J.H.M.L.C.; Chakthranont, P.; Vojvodic, A.; Jaramillo, T.F.; Nørskov, J.K. Materials for solar fuels and chemicals. *Nat. Mater.* **2017**, *16*, 70–81. [[CrossRef](#)]
7. Prévot, M.S.; Sivula, K. Photoelectrochemical Tandem Cells for Solar Water Splitting. *J. Phys. Chem. C* **2013**, *117*, 17879–17893. [[CrossRef](#)]
8. Higashi, T.; Kaneko, H.; Minegishi, T.; Kobayashi, H.; Zhong, M.; Kuang, Y.; Hisatomi, T.; Katayama, M.; Takata, T.; Nishiyama, H.; et al. Overall water splitting by photoelectrochemical cells consisting of (ZnSe)_{0.85}(CuIn_{0.7}Ga_{0.3}Se₂)_{0.15} photocathodes and BiVO₄ photoanodes. *Chem. Commun.* **2017**, *53*, 11674–11677. [[CrossRef](#)]
9. Higashi, T.; Shinohara, Y.; Ohnishi, A.; Liu, J.; Ueda, K.; Okamura, S.; Hisatomi, T.; Katayama, M.; Nishiyama, H.; Yamada, T.; et al. Sunlight-Driven Overall Water Splitting by the Combination of Surface-Modified La₅Ti₂Cu_{0.9}Ag_{0.1}S₅O₇ and BaTaO₂N Photoelectrodes. *ChemPhotoChem* **2017**, *1*, 167–172. [[CrossRef](#)]
10. Kaneko, H.; Minegishi, T.; Nakabayashi, M.; Shibata, N.; Kuang, Y.; Yamada, T.; Domen, K. A Novel Photocathode Material for Sunlight-Driven Overall Water Splitting: Solid Solution of ZnSe and Cu(In,Ga)Se₂. *Adv. Funct. Mater.* **2016**, *26*, 4570–4577. [[CrossRef](#)]
11. Hisatomi, T.; Okamura, S.; Liu, J.; Shinohara, Y.; Ueda, K.; Higashi, T.; Katayama, M.; Minegishi, T.; Domen, K. La₅Ti₂Cu_{1-x}Ag_xS₅O₇ photocathodes operating at positive potentials during photoelectrochemical hydrogen evolution under irradiation of up to 710 nm. *Energy Environ. Sci.* **2015**, *8*, 3354–3362. [[CrossRef](#)]
12. Song, A.; Bogdanoff, P.; Esau, A.; Ahmet, I.Y.; Levine, I.; Dittrich, T.; Unold, T.; van de Krol, R.; Berglund, S.P. Assessment of a W:BiVO₄-CuBi₂O₄ Tandem Photoelectrochemical Cell for Overall Solar Water Splitting. *ACS Appl. Mater. Interfaces* **2020**, *12*, 13959–13970. [[CrossRef](#)]
13. Kobayashi, H.; Sato, N.; Orita, M.; Kuang, Y.; Kaneko, H.; Minegishi, T.; Yamada, T.; Domen, K. Development of highly efficient CuIn_{0.5}Ga_{0.5}Se₂-based photocathode and application to overall solar driven water splitting. *Energy Environ. Sci.* **2018**, *11*, 3003–3009. [[CrossRef](#)]
14. Huang, D.; Wang, K.; Li, L.; Feng, K.; An, N.; Ikeda, S.; Kuang, Y.; Ng, Y.; Jiang, F. 3.17% efficient Cu₂ZnSnS₄-BiVO₄ integrated tandem cell for standalone overall solar water splitting. *Energy Environ. Sci.* **2021**, *14*, 1480–1489. [[CrossRef](#)]
15. Jiang, F.; Harada, T.; Kuang, Y.; Minegishi, T.; Domen, K.; Ikeda, S. Pt/In₂S₃/CdS/Cu₂ZnSnS₄ Thin Film as an Efficient and Stable Photocathode for Water Reduction under Sunlight Radiation. *J. Am. Chem. Soc.* **2015**, *137*, 13691–13697. [[CrossRef](#)] [[PubMed](#)]
16. Kim, J.H.; Kaneko, H.; Minegishi, T.; Kubota, J.; Domen, K.; Lee, J.S. Overall Photoelectrochemical Water Splitting using Tandem Cell under Simulated Sunlight. *ChemSusChem* **2016**, *9*, 61–66. [[CrossRef](#)]
17. Chun, W.-J.; Ishikawa, A.; Fujisawa, H.; Takata, T.; Kondo, J.N.; Hara, M.; Kawai, M.; Matsumoto, A.Y.; Domen, K. Conduction and Valence Band Positions of Ta₂O₅, TaON, and Ta₃N₅ by UPS and Electrochemical Methods. *J. Phys. Chem. B* **2003**, *107*, 1798–1803. [[CrossRef](#)]
18. Higashi, M.; Domen, K.; Abe, R. Fabrication of efficient TaON and Ta₃N₅ photoanodes for water splitting under visible light irradiation. *Energy Environ. Sci.* **2011**, *4*, 4138–4147. [[CrossRef](#)]
19. Pinaud, B.A.; Vesborg, P.C.K.; Jaramillo, T.F. Effect of Film Morphology and Thickness on Charge Transport in Ta₃N₅/Ta Photoanodes for Solar Water Splitting. *J. Phys. Chem. C* **2012**, *116*, 15918–15924. [[CrossRef](#)]
20. Liu, G.; Ye, S.; Yan, P.; Xiong, F.; Fu, P.; Wang, Z.; Chen, Z.; Shi, J.; Li, C. Enabling an integrated tantalum nitride photoanode to approach the theoretical photocurrent limit for solar water splitting. *Energy Environ. Sci.* **2016**, *9*, 1327–1334. [[CrossRef](#)]
21. Takanabe, K. Photocatalytic Water Splitting: Quantitative Approaches toward Photocatalyst by Design. *ACS Catal.* **2017**, *7*, 8006–8022. [[CrossRef](#)]
22. Jing, T.; Dai, Y.; Ma, X.; Wei, W.; Huang, B. Effects of intrinsic defects and extrinsic doping on the electronic and photocatalytic properties of Ta₃N₅. *RSC Adv.* **2015**, *5*, 59390–59397. [[CrossRef](#)]
23. Fu, G.; Yan, S.; Yu, T.; Zou, Z. Oxygen related recombination defects in Ta₃N₅ water splitting photoanode. *Appl. Phys. Lett.* **2015**, *107*, 171902. [[CrossRef](#)]
24. Harb, M.; Sautet, P.; Nurlaela, E.; Raybaud, P.; Cavallo, L.; Domen, K.; Basset, J.-M.; Takanabe, K. Tuning the properties of visible-light-responsive tantalum (oxy)nitride photocatalysts by non-stoichiometric compositions: A first-principles viewpoint. *Phys. Chem. Chem. Phys.* **2014**, *16*, 20548–20560. [[CrossRef](#)] [[PubMed](#)]

25. Nurlaela, E.; Ould-Chikh, S.; Harb, M.; Del Gobbo, S.; Aouine, M.; Puzenat, E.; Sautet, P.; Domen, K.; Basset, J.-M.; Takanabe, K. Critical Role of the Semiconductor–Electrolyte Interface in Photocatalytic Performance for Water-Splitting Reactions Using Ta₃N₅ Particles. *Chem. Mater.* **2014**, *26*, 4812–4825. [[CrossRef](#)]
26. Murthy, D.H.K.; Matsuzaki, H.; Wang, Z.; Suzuki, Y.; Hisatomi, T.; Seki, K.; Inoue, Y.; Domen, K.; Furube, A. Origin of the overall water splitting activity of Ta₃N₅ revealed by ultrafast transient absorption spectroscopy. *Chem. Sci.* **2019**, *10*, 5353–5362. [[CrossRef](#)]
27. Ziani, A.; Nurlaela, E.; Dhawale, D.S.; Silva, D.A.; Alarousu, E.; Mohammed, O.F.; Takanabe, K. Carrier dynamics of a visible-light-responsive Ta₃N₅ photoanode for water oxidation. *Phys. Chem. Chem. Phys.* **2014**, *17*, 2670–2677. [[CrossRef](#)] [[PubMed](#)]
28. Li, M.; Luo, W.; Cao, D.; Zhao, X.; Li, Z.; Yu, T.; Zou, Z. A Co-catalyst-Loaded Ta₃N₅ Photoanode with a High Solar Photocurrent for Water Splitting upon Facile Removal of the Surface Layer. *Angew. Chem. Int. Ed.* **2013**, *52*, 11016–11020. [[CrossRef](#)] [[PubMed](#)]
29. Shao, C.; Chen, R.; Zhao, Y.; Li, Z.; Zong, X.; Li, C. Reducing the surface defects of Ta₃N₅ photoanode towards enhanced photoelectrochemical water oxidation. *J. Mater. Chem. A* **2020**, *8*, 23274–23283. [[CrossRef](#)]
30. Wang, L.; Zhou, X.; Nguyen, N.T.; Hwang, I.; Schmuki, P. Strongly Enhanced Water Splitting Performance of Ta₃N₅ Nanotube Photoanodes with Subnitrides. *Adv. Mater.* **2016**, *28*, 2432–2438. [[CrossRef](#)] [[PubMed](#)]
31. Liao, M.; Feng, J.; Luo, W.; Wang, Z.; Zhang, J.; Li, Z.; Yu, T.; Zou, Z. Co₃O₄ Nanoparticles as Robust Water Oxidation Catalysts Towards Remarkably Enhanced Photostability of a Ta₃N₅ Photoanode. *Adv. Funct. Mater.* **2012**, *22*, 3066–3074. [[CrossRef](#)]
32. Hou, J.; Wang, Z.; Yang, C.; Cheng, H.; Jiao, S.; Zhu, H. Cobalt-bilayer catalyst decorated Ta₃N₅ nanorod arrays as integrated electrodes for photoelectrochemical water oxidation. *Energy Environ. Sci.* **2013**, *6*, 3322–3330. [[CrossRef](#)]
33. Suzuki, S.; Yanai, M.; Yamada, T.; Wagata, H.; Sasaki, Y.; Oishi, S.; Domen, K.; Teshima, K. Ta₃N₅ Photoanodes Fabricated by Providing NaCl–Na₂CO₃ Evaporants to Tantalum Substrate Surface under NH₃ Atmosphere. *ACS Appl. Energy Mater.* **2018**, *1*, 6129–6135. [[CrossRef](#)]
34. Zhong, M.; Hisatomi, T.; Sasaki, Y.; Suzuki, S.; Teshima, K.; Nakabayashi, M.; Shibata, N.; Nishiyama, H.; Katayama, M.; Yamada, T.; et al. Highly Active GaN-Stabilized Ta₃N₅ Thin-Film Photoanode for Solar Water Oxidation. *Angew. Chem. Int. Ed.* **2017**, *56*, 4739–4743. [[CrossRef](#)]
35. Wang, Z.; Qi, Y.; Ding, C.; Fan, D.; Liu, G.; Zhao, Y.; Li, C. Insight into the charge transfer in particulate Ta₃N₅ photoanode with high photoelectrochemical performance. *Chem. Sci.* **2016**, *7*, 4391–4399. [[CrossRef](#)] [[PubMed](#)]
36. Liu, G.; Fu, P.; Zhou, L.; Yan, P.; Ding, C.; Shi, J.; Li, C. Efficient Hole Extraction from a Hole-Storage-Layer-Stabilized Tantalum Nitride Photoanode for Solar Water Splitting. *Chem. A Eur. J.* **2015**, *21*, 9624–9628. [[CrossRef](#)] [[PubMed](#)]
37. Haleem, A.A.; Majumder, S.; Perumandla, N.; Zahran, Z.N.; Naruta, Y. Enhanced Performance of Pristine Ta₃N₅ Photoanodes for Solar Water Splitting by Modification with Fe–Ni–Co Mixed-Metal Oxide Cocatalysts. *J. Phys. Chem. C* **2017**, *121*, 20093–20100. [[CrossRef](#)]
38. Haleem, A.A.; Perumandla, N.; Naruta, Y. Preparation of Nanostructured Ta₃N₅ Electrodes by Alkaline Hydrothermal Treatment Followed by NH₃ Annealing and Their Improved Water Oxidation Performance. *ACS Omega* **2019**, *4*, 7815–7821. [[CrossRef](#)]
39. Seo, J.; Takata, T.; Nakabayashi, M.; Hisatomi, T.; Shibata, N.; Minegishi, T.; Domen, K. Mg–Zr Cosubstituted Ta₃N₅ Photoanode for Lower-Onset-Potential Solar-Driven Photoelectrochemical Water Splitting. *J. Am. Chem. Soc.* **2015**, *137*, 12780–12783. [[CrossRef](#)] [[PubMed](#)]
40. Akagi, D.; Kageshima, Y.; Hashizume, Y.; Aoi, S.; Sasaki, Y.; Kaneko, H.; Higashi, T.; Hisatomi, T.; Katayama, M.; Minegishi, T.; et al. A Semitransparent Nitride Photoanode Responsive up to λ = 600 nm Based on a Carbon Nanotube Thin Film Electrode. *ChemPhotoChem* **2019**, *3*, 521–524. [[CrossRef](#)]
41. Kim, Y.W.; Cha, S.; Kwak, I.; Kwon, I.S.; Park, K.; Jung, C.S.; Cha, E.H.; Park, J. Surface-Modified Ta₃N₅ Nanocrystals with Boron for Enhanced Visible-Light-Driven Photoelectrochemical Water Splitting. *ACS Appl. Mater. Interfaces* **2017**, *9*, 36715–36722. [[CrossRef](#)] [[PubMed](#)]
42. Nurlaela, E.; Shinagawa, T.; Qureshi, M.; Dhawale, D.S.; Takanabe, K. Temperature Dependence of Electrocatalytic and Photocatalytic Oxygen Evolution Reaction Rates Using NiFe Oxide. *ACS Catal.* **2016**, *6*, 1713–1722. [[CrossRef](#)]
43. Higashi, T.; Nishiyama, H.; Otsuka, Y.; Kawase, Y.; Sasaki, Y.; Nakabayashi, M.; Katayama, M.; Minegishi, T.; Shibata, N.; Takanabe, K.; et al. Efficient Water Oxidation Using Ta₃N₅ Thin Film Photoelectrodes Prepared on Insulating Transparent Substrates. *ChemSusChem* **2020**, *13*, 1974–1978. [[CrossRef](#)]
44. Higashi, T.; Nishiyama, H.; Suzuki, Y.; Sasaki, Y.; Hisatomi, T.; Katayama, M.; Minegishi, T.; Seki, K.; Yamada, T.; Domen, K. Transparent Ta₃N₅ Photoanodes for Efficient Oxygen Evolution toward the Development of Tandem Cells. *Angew. Chem. Int. Ed.* **2019**, *58*, 2300–2304. [[CrossRef](#)]
45. Smith, R.D.L.; Prévot, M.S.; Fagan, R.D.; Zhang, Z.; Sedach, P.A.; Siu, M.K.J.; Trudel, S.; Berlinguette, C.P. Photochemical Route for Accessing Amorphous Metal Oxide Materials for Water Oxidation Catalysis. *Science* **2013**, *340*, 60–63. [[CrossRef](#)]
46. McCrory, C.C.L.; Jung, S.; Peters, J.C.; Jaramillo, T.F. Benchmarking Heterogeneous Electrocatalysts for the Oxygen Evolution Reaction. *J. Am. Chem. Soc.* **2013**, *135*, 16977–16987. [[CrossRef](#)]
47. Kawase, Y.; Higashi, T.; Katayama, M.; Domen, K.; Takanabe, K. Maximizing Oxygen Evolution Performance on a Transparent NiFeO_x/Ta₃N₅ Photoelectrode Fabricated on Insulating Quartz Substrates. *ACS Appl. Mater. Interfaces* **2021**, *13*, 16317–16325. [[CrossRef](#)] [[PubMed](#)]
48. Minegishi, T.; Nishimura, N.; Kubota, J.; Domen, K. Photoelectrochemical properties of LaTiO₂N electrodes prepared by particle transfer for sunlight-driven water splitting. *Chem. Sci.* **2012**, *4*, 1120–1124. [[CrossRef](#)]